Current–Voltage Relations and Steady-State Characteristics of Na^+–Ca^{2+} Exchange: Characterization of the Eight-State Consecutive Transport Model

Alexander Omelchenko and Larry V. Hryshko
Institute of Cardiovascular Sciences, St. Boniface General Hospital Research Centre, University of Manitoba, Winnipeg, Manitoba R2H 2A6, Canada

ABSTRACT An analytical expression for Na^+–Ca^{2+} exchange currents in cardiac cells has been obtained for an eight-state model. The equation obtained has been used to derive theoretical expressions for current–voltage relationships, maximum Na^+–Ca^{2+} exchange currents, and half-saturating concentrations for Na^+ and Ca^{2+}. These equations were analyzed over a wide range of cytoplasmic and extracellular Na^+ and Ca^{2+} concentrations, under forward and reverse "zero-*trans*" conditions. Correspondence of theoretical results with those obtained from giant excised patch experiments are presented. Rate constants from published reports were used to evaluate turnover rates for Na^+–Ca^{2+} exchange in the forward and reverse directions. A factor, ε, is introduced that permits prediction of the extent to which the Na^+–Ca^{2+} exchange cycle is under voltage or diffusion control. This factor can be conveniently used for data interpretation and comparison. The derived equations also provide a foundation for continuing experimental evaluation of the fidelity of this model.

INTRODUCTION

Na^+–Ca^{2+} exchange is an electrogenic process with a stoichiometry of 3 Na^+:1 Ca^{2+} (for review, see Philipson and Nicoll, 1993). Recent evidence suggests that the exchanger transports Na^+ and Ca^{2+} in separate consecutive steps and that the movement of one positive charge is associated with Na^+ translocation (Hilgemann et al., 1991; Matsuoka and Hilgemann, 1992). An eight-state consecutive transport model describing Na^+–Ca^{2+} exchange was introduced by Hilgemann et al. (1991) that is similar to the Post–Albers scheme describing the behavior of the Na, K pump (Post et al., 1972). Within the framework of this model, the exchanger's ion-binding sites reorient between the cytoplasmic and the extracellular sides only when they are loaded with 3 Na^+ or 1 Ca^{2+}. Transitional states with occluded Na^+ and Ca^{2+} are assumed. Both occlusion and deocclusion reactions for Na^+ ions are treated as single-step reactions. All ion-binding reactions are treated as voltage-independent, instantaneous equilibria. Electrogenicity is associated with occlusion–deocclusion of Na^+ into or from the transport complex, or with Na^+ unbinding from the complex on the extracellular side, or both. This model represents the minimum complexities of the transport cycle and does not account for cytoplasmic Na^+ and Ca^{2+} regulation (Hilgemann, 1990). Thus, analysis is restricted to consideration of the transport properties of the deregulated Na^+–Ca^{2+} exchanger.

Such an analysis involving detailed studies of ion and voltage dependencies of Na^+–Ca^{2+} exchange was undertaken by Matsuoka and Hilgemann (1992). They demonstrated 1) changes of apparent ion affinities in response to changes of countertransported ion concentrations, 2) shape changes of current–voltage (I–V) relationships for inward and outward Na^+–Ca^{2+} exchange current owing to changes in both Na^+ and Ca^{2+} concentrations, and 3) shape changes of outward and inward I–V relationships with inhibition by the countertransported ion from the cytoplasmic side. To explain these results, three models were introduced that could account for all observed Na^+–Ca^{2+} exchange current characteristics. The common, minimal requirements for these consecutive exchange models were 1) multiple voltage- and time-dependent occlusion–deocclusion steps in the Na^+ transport pathway, 2) a small voltage dependence of Ca^{2+} occlusion–deocclusion on the cytoplasmic side, and 3) the existence of a site that could bind one Ca^{2+} and one Na^+ ion on the cytoplasmic side (Matsuoka and Hilgemann, 1992). The eight-state model originally proposed (Hilgemann et al., 1991) does not share these requirements.

All four models could be fitted reasonably well to the experimental data. Thus, fitting procedures alone cannot be used to determine the appropriateness of the model at the microscopic level. At the same time, despite its complexity, the mathematical analysis of the voltage and concentration dependencies of ion fluxes can yield detailed information on the microscopic properties of an ion transport system and establish experimental criteria for the distinction among various models (Lauger, 1972, 1987; Markin and Chizmadjev, 1974). It should be noted that such mathematical analysis reveals intrinsic features of the model, independently of chosen numerical values for rate constants.

The objectives of the present study were to investigate theoretically the intrinsic features inherent in the eight-state model. Numerical examples based on designated values of rate and binding constants are given to compare them with existing experimental data.

Received for publication 1 April 1996 and in final form 2 July 1996.

Address reprint requests to Dr. Alexander Omelchenko, Institute of Cardiovascular Sciences, St. Boniface Hospital Research Centre, R3032, 351 Tache Avenue, Winnepeg, Manitoba R2H 2A6, Canada. Tel.: 204-235-3662; Fax: 204-233-6723; E-mail: lhryshko@brc.umanitoba.ca.

0006-3495/96/10/1751/13 $2.00

MODEL DESCRIPTION

The scheme of the consecutive (or Ping-Pong) Na^+–Ca^{2+} exchange cycle proposed by Hilgemann et al. (1991) is presented in Fig. 1 with slight modification. Here, rate constants are designated by subscripts indicating the directions of transitions. They are pseudomonomolecular rate constants (expressed in s^{-1}) that may include ion concentration and may depend on voltage (Lauger, 1991). For outward Na^+ translocation coupled to inward Ca^{2+} transport the following eight steps are assumed: 1) binding of three Na^+ ions to the unloaded exchanger protein in the inward-facing configuration, 2) simultaneous occlusion of bound Na^+ inside the exchanger, 3) simultaneous deocclusion of bound Na^+ during which the exchanger transfers to a new conformational state with outward-facing binding sites, 4) release of Na^+ to the extracellular side, 5) binding of one Ca^{2+} ion to the unloaded exchanger in an outward-facing configuration, 6) occlusion of Ca^{2+} inside the exchanger, 7) deocclusion of Ca^{2+} and a conformational shift to inward-facing binding sites, and 8) release of Ca^{2+} to the cytoplasm.

The mathematical route for obtaining the general solution for Na^+–Ca^{2+} exchange current and the assignment of rate constants are presented in the Appendix. Although the general solution is quite cumbersome, it can be simplified considerably by the use of "zero-*trans*" conditions. As Na^+–Ca^{2+} exchange is generally considered a Ca^{2+} efflux mechanism using Na^+ influx as the driving force, we consider the "forward zero-*trans*" condition to represent vanishing cytoplasmic Na^+ and extracellular Ca^{2+} concentrations. Opposite conditions are considered "reverse zero-*trans*." Expressions for both outward and inward I–V relationships are shown in the Appendix.

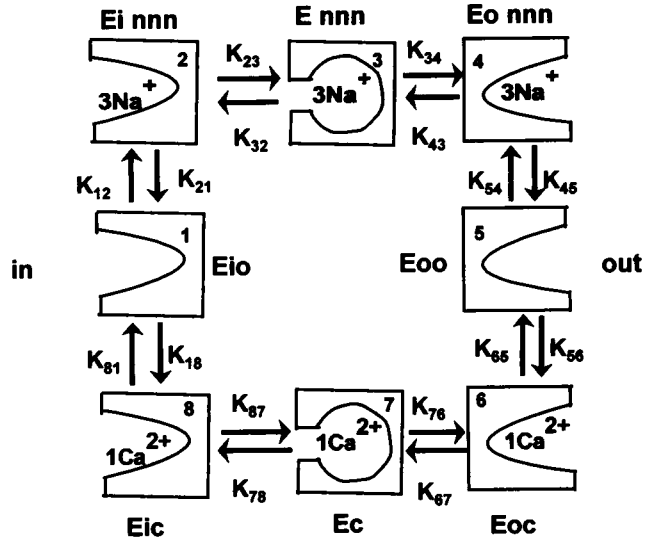

FIGURE 1 Schematic representation of the Na^+–Ca^{2+} exchange transport cycle. States with binding sites facing the cytoplasm are designated E_i states, whereas those with binding sites facing the extracellular side are designated E_o states. E_{io} and E_{oo} are unloaded states. E_{innn} and E_{onnn} are 3 Na^+ loaded states, E_{ic} and E_{oc} are 1 Ca^{2+} loaded states, and E_{nnn} and E_c are transitional states with "occluded" Na^+ and Ca^{2+}, respectively.

STEADY-STATE FEATURES OF THE TRANSPORT MODEL AND COMPARISON WITH EXPERIMENTAL RESULTS

"Reverse zero-*trans*" conditions ($N_o = 0$, $C_i = 0$)

Current–voltage relations and maximum turnover rates

Equation A6 of the Appendix can be rewritten, in terms of dependence on f_{co}, f_{3ni}, and Ψ, as

$$I_o = \frac{a_1 f_{co} f_{3ni} e^{\Psi/2}}{(a_2 + a_3 f_{3ni}) f_{co} + [(a_4 + a_5 f_{3ni}) f_{co} + a_6 f_{3ni}] e^{\Psi/2}}, \quad (1)$$

where a_1–a_6 are constants:

$$a_1 = e_o X k_{ci} k_{co} k_{ni} k_{no} l'_{co} l'_{ni} l''_{ci} l''_{no}, \qquad a_2 = 3 k_{ci} k_{co} k_{ni} k_{no} l'_{co} l''_{ci} l''_{ni},$$

$$a_3 = k_{ci} k_{co} k_{ni} k_{no} l'_{co} l'_{ni} l''_{ci}, \qquad a_4 = 3 k_{ci} k_{co} k_{ni} k_{no} l'_{co} l''_{ci} l''_{no},$$

$$a_5 = [(k_{ci} k_{no} + k_{ci} l''_{ci} + k_{no} l''_{ci}) k_{co} k_{ni} + 2(k_{co} + k_{ni}) k_{ci} k_{no} l''_{ci}] l'_{co} l'_{ni} l''_{no},$$

$$a_6 = 3(l''_{ci} + l''_{co}) k_{ci} k_{co} k_{ni} k_{no} l'_{ni} l''_{no}.$$

Outward I–V relations at different C_o and N_i calculated from Eq. 1 are presented in Fig. 2. These are consistent with experimental data (Matsuoka and Hilgemann, 1992). Formally, at $l''_{no} \gg l''_{ci}$ and $l''_{no} \gg l''_{ni}$, shielding of membrane potential can take place at $\Psi > 0$, and exchange current becomes voltage independent. This is not a result attributable to the selected numerical values of rate constants but, rather, is inherent in the model. At small l''_{no}, I_o can exhibit an exponential dependence on Ψ. An exponential behavior of Na^+-dependent Ca^{2+} influx into cardiac sarcolemmal vesicles has been observed for voltages between −60 and +140 mV (Ledvora and Hegyvary, 1983).

I_o is an increasing function of C_o and N_i and saturates as both C_o and $N_i \to \infty$. At strongly hyperpolarizing voltages ($\Psi \to -\infty$), $I_o = 0$ for any C_o and N_i. This is consistent with findings that reduction of C_o causes a remarkable decrease of I_o at positive potentials, whereas the current at −120 mV hardly decreases at all (Matsuoka and Hilgemann, 1992).

It can be seen from Eq. 1 that reduction of C_o, while keeping N_i at comparatively high levels, causes a complete loss of voltage dependence of I_o at intermediate potentials. In this case, I_o does not depend on Na^+ transport characteristics, and Eq. 1 yields

$$I_o = e_o X L_{co} f_{co}. \quad (2)$$

Equation 2 describes outward exchange current, provided that the following two conditions of Ca_o exhaustion are met:

$$\frac{1}{f_{co}} \gg \frac{L_{co}}{3}\left(\frac{1}{k_{ci}} + \frac{1}{k_{no}} + \frac{1}{l''_{ci}} + \frac{2}{k_{co}} + \frac{2}{k_{ni}} + \frac{3}{l'_{ni} f_{3ni}}\right), \quad (3)$$

$$\frac{1}{f_{co}} \gg \frac{L_{co}}{l''_{no}}\left(\frac{1}{3} + \frac{l''_{ni}}{l'_{ni} f_{3ni}}\right). \quad (4)$$

Note that conditions 3 and 4 depend on cytoplasmic Na^+, but decreasing N_i alone does not cause a loss of voltage dependence of I_o. Calculations according to condition 3 yield $C_o \ll 0.1$ mM and $C_o \ll 5.5$ mM and to condition 4 yield $C_o \ll 0.1$ mM and $C_o \ll 2.7$ mM for 8 and 100 mM N_i, respectively. Here, condition 4 overlaps condition 3. Nearly complete loss of voltage dependence with 0.1–0.2 mM C_o (and less) at 100 mM N_i was observed experimen-

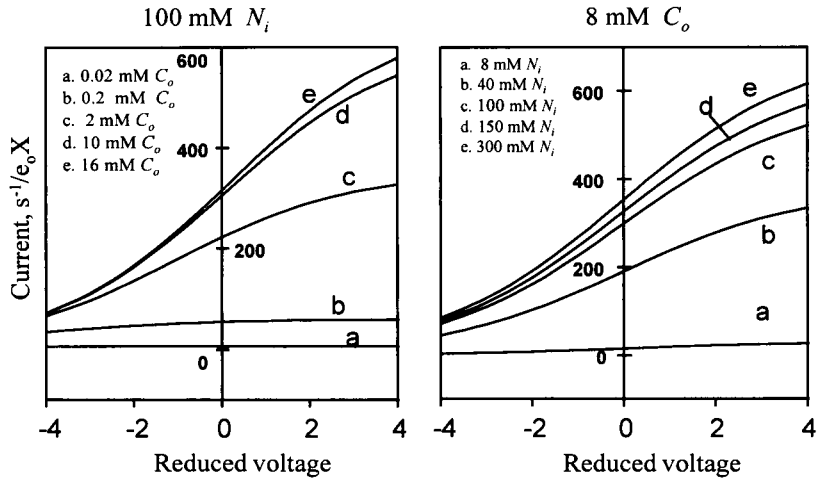

FIGURE 2 Dependence of outward I–V relations on C_o and N_i. Here, reduced voltage $\Psi \sim E_m/25$ mV (see text for details).

tally (Hilgemann et al., 1991; Matsuoka and Hilgemann, 1992). This loss reflects the electrically silent character of Ca^{2+} transport, which becomes rate limiting as C_o is substantially reduced. Under the same experimental conditions a small negative slope was occasionally observed with depolarization (Hilgemann et al., 1991). Note that this nonmonotonic behavior of I_o can take place only if Ca^{2+}-loaded transport complexes bear at least a fraction of charge (Lauger, 1987; Niggli and Lederer, 1991; Hilgemann et al., 1991). However, a negative slope of I–V relations has not been obtained in other, more recent experimental series (Matsuoka and Hilgemann, 1992). Clearly, additional studies are required to assess this possibility.

Exchange current is an increasing function of membrane voltage and saturates with strong depolarization (i.e., as $\Psi \to \infty$):

$$I_{\max,\Psi\to\infty} = \frac{a_1 f_{co} f_{3ni}}{[(a_4+a_5 f_{3ni})f_{co}+a_6 f_{3ni}]}. \quad (5)$$

Note that $I_{\max,\Psi\to\infty}$ does not depend on the intrinsic Na^+ deocclusion rate constant for the extracellular side, l''_{no}. From Eq. A7 below, the maximum outward turnover rate, ν_o, can be defined as Ψ and the concentrations of transported ions approach infinity (i.e., as $f_{3ni} = f_{co} = 1$):

$$\nu_{o,\max} = \left(\frac{1}{k_{ci}} + \frac{1}{k_{no}} + \frac{1}{l''_{ci}} + \frac{2}{k_{co}} + \frac{2}{k_{ni}} + \frac{3}{l'_{ni}} + \frac{3}{L_{co}}\right)^{-1}.$$

Using the above values of rate constants, we find that $\nu_o \cong 1000\ s^{-1}$. A maximum outward turnover rate under short-circuit conditions (i.e., $\Psi = 0$) is given by

$$\nu_{o,s.c.} = \left(\frac{1}{k_{ci}} + \frac{1}{k_{no}} + \frac{1}{l''_{ci}} + \frac{1}{l''_{no}} + \frac{2}{k_{co}} + \frac{2}{k_{ni}} + \frac{3}{L_{co}} + \frac{3}{L_{ni}}\right)^{-1}.$$

$\nu_{o,s.c.}$ is calculated to be $\cong 430\ s^{-1}$, i.e., less than half of that at infinite depolarization.

Generally, $I_{\max,\Psi\to\infty}$ depends on both N_i and C_o. Both I_o and $I_{\max,\Psi\to\infty}$ are independent of C_o if conditions opposite conditions 3 and 4 are met. Here, conditions of Ca_o exhaustion are replaced by conditions of Ca_o saturation. Experimental data on Ca_o saturation of I_o are limited. I_o shows a saturation tendency at $C_o > 1.2$ mM in the presence of 100 mM N_i (Matsuoka and Hilgemann, 1992). The Ca_o-saturating concentration decreases as N_i is reduced. At the same time, $I_{\max,\Psi\to\infty}$ is independent of N_i if the condition of Na_i saturation (i.e., $f_{3ni} \gg a_4/a_5$) is fulfilled. In terms of rate constants, this reads as

$$\frac{1}{f_{3ni}} \ll \frac{l'_{ni}}{3}\left(\frac{1}{k_{ci}} + \frac{1}{k_{no}} + \frac{1}{l''_{ci}} + \frac{2}{k_{co}} + \frac{2}{k_{ni}}\right),$$

and N_i is calculated to be very high, namely, at $N_i \gg 500$ mM. This limitation cannot easily be tested under experimental conditions, but it is interesting that the condition of Na_i saturation does not depend on C_o. This means that Na_i saturation cannot be approached if N_i does not exceed a certain value (here, 500 mM with the above values of rate constants) at any C_o.

Effect of ion concentration on the shape of outward I–V relations

The slope of outward I–V relations is given by

$$\frac{dI_o}{d\Psi} = \frac{a_1(a_2+a_3 f_{3ni}) f_{co}^2 f_{3ni} e^{\Psi/2}}{\{[(a_4+a_5 f_{3ni})f_{co}+a_6 f_{3ni}]e^{\Psi/2}+(a_2+a_3 f_{3ni})f_{co}\}^2}. \quad (6)$$

The C_o dependence of the outward I–V relation slope calculated from Eq. 6 at $\Psi = 0$ is presented in Fig. 3. Practically, the slope does not depend on C_o in the range 1–6 mM at low concentrations of cytoplasmic Na^+ (i.e., <8 mM). Apparently, this reflects Ca_o saturation as cytoplasmic Na^+ is reduced to 8 mM (and less). The slope of I–V relations increases as C_o is increased at elevated N_i.

Significantly reduced C_o can also affect the dependence of outward I–V relations on N_i. Equation 6 reveals the critical fraction $\tilde{f}_{3ni}$ and the critical cytoplasmic Na^+ con-

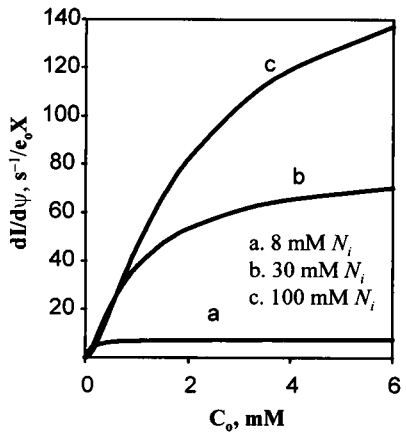

FIGURE 3 Dependence of the slope of outward I–V relations on C_o at different values of N_i. $\Psi = 0$.

centration $\tilde{N}_i$ for the dependence of I–V relation slope on N_i, given, respectively, by

$$\tilde{f}_{3ni} = \frac{a_2(a_2+a_4)f_{co}}{a_2a_6 - [(a_2 + 2a_4)a_3 - a_2a_5]f_{co}}, \qquad \tilde{N}_i = \frac{K_{ni}\tilde{f}_{3ni}^{1/3}}{1-\tilde{f}_{3ni}^{1/3}}.$$

Calculated dependencies of I–V relation slopes on N_i at different C_o are shown in Fig. 4. At low N_i the slope increases as N_i is increased. Then the slope slowly decreases if N_i exceeds ~16 mM at a C_o of 0.2 mM, or if it exceeds ~30 mM at a C_o of 0.5 mM. Increasing C_o above 1.2 mM sharply eliminates this critical influence of N_i.

Experiments that use nonsaturating concentrations of both N_i and C_o simultaneously are few. From the available data (Matsuoka and Hilgemann, 1992) it can be noted that the slope of the outward I–V increases as 1) N_i is increased from 6 mM to 100 mM (with saturation tendency above 50 mM) at 8 mM C_o and 2) as C_o is increased from 0.2 mM to 10 mM at 100 mM N_i. The calculated dependencies are compatible with these experimental findings.

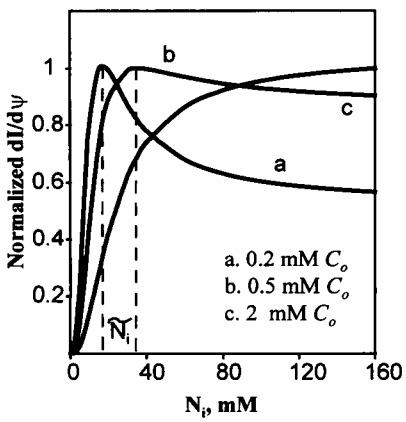

FIGURE 4 Dependence of the slope of outward I–V relations on N_i at different values of C_o. $\Psi = 0$. Data for each curve are normalized to their corresponding maximum value.

The curvature of I–V relations is determined by

$$\frac{d^2I_o}{d\Psi^2} = \frac{x_1(x_3 - x_2e^{\Psi/2})e^{\Psi/2}}{4(x_3+x_2e^{\Psi/2})^3},$$

where $x_1 = a_1(a_2 + a_3f_{3ni})f_{co}^2f_{3ni}$, $x_2 = a_6f_{3ni} + (a_4 + a_5f_{3ni})f_{co}$, and $x_3 = (a_2 + a_3f_{3ni})f_{co}$. Highly positive potentials favor convex I–V relations, whereas strongly negative potentials produce concave patterns. This means that I–V relations have a tendency to saturate at extreme depolarization and hyperpolarization levels. At intermediate potentials, I–V relations can be convex or concave, depending on C_o and N_i. The potential of inflection, $\tilde{\Psi}$, is given by

$$\tilde{\Psi} = 2\ln(x_3/x_2). \tag{7}$$

The potential of inflection decreases as C_o is reduced, and, at small f_{co}, $\tilde{\Psi} \to -\infty$. This means that, at low C_o, I–V relations will be convex at every Ψ, consistent with experimental data showing outward I–V relations progressively flattening at intermediate potentials as C_o is reduced (Hilgemann et al., 1991).

The potential of inflection at low N_i is calculated to be $\cong 0$ mV at $l''_{ni} \cong l''_{no}$. In contrast to the C_o effect, $\tilde{\Psi}$ can be either an increasing or a decreasing function of N_i depending on C_o, and from Eq. 7, $\tilde{\Psi}$ is a decreasing function of N_i if the following condition is met:

$$\frac{1}{f_{co}} > \frac{L_{co}}{3}\left(\frac{1}{l''_{ni}} - \frac{1}{k_{ci}} - \frac{1}{k_{no}} - \frac{1}{l''_{ci}} - \frac{2}{k_{co}} - \frac{2}{k_{ni}}\right). \tag{8}$$

The value in parentheses must always be positive; otherwise the cycle will rotate in the opposite direction, which is inconsistent with an outward current. Condition 8 can be realized at $C_o < \bar{C}_o$, where $\bar{C}_o$ is a critical extracellular Ca^{2+} concentration for the dependence of $\tilde{\Psi}$ on N_i, and is given by

$$\bar{C}_o = \frac{K_{co}}{\frac{L_{co}}{3}\left(\frac{1}{l''_{ni}} - \frac{1}{k_{ci}} - \frac{1}{k_{no}} - \frac{1}{l''_{ci}} - \frac{2}{k_{co}} - \frac{2}{k_{ni}}\right) - 1}. \tag{9}$$

With the selected values of rate constants (Appendix), one finds that $\bar{C}_o \cong 12$ mM. This indicates that, if $C_o < 12$ mM, the inflection potential $\tilde{\Psi}$ for I–V relations increases as N_i is decreased. This result is compatible with experimental data showing that outward I–V relations progressively flatten, except at very negative and very positive potentials, as N_i is increased and that the current gains in steepness as N_i is reduced from 100 mM to 8 mM (Matsuoka and Hilgemann, 1992; Doering et al., 1996). Thus, the role of extracellular Ca^{2+} concentration should be taken into account during data interpretation. Otherwise, the effect of N_i reduction can be attributed to altered Na^+ rate constants on the cytoplasmic side. If $C_o > 12$ mM, the inflection potential decreases and I–V curves flatten as N_i is reduced. Calculated I–V curves for C_o below and above $\bar{C}_o$ are presented in Fig. 5. Inasmuch as high C_o weakly affects the slope of I–V relations (Fig. 3), the effect of N_i cannot be clearly seen in Fig.

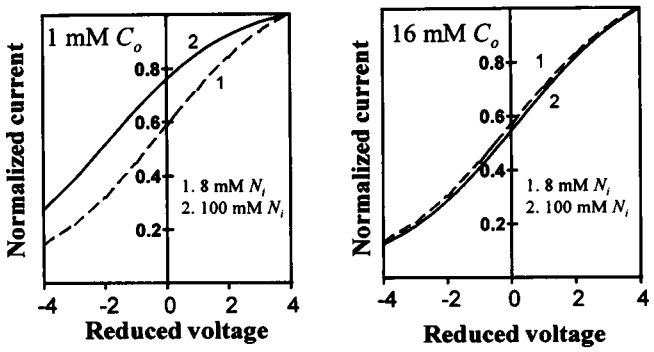

FIGURE 5 Dependence of outward I–V relations on N_i at 1- and 16-mM C_o. Data are normalized to the amplitude at 100 mV.

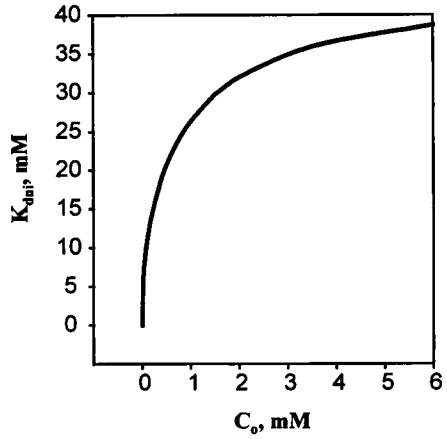

FIGURE 6 Dependence of half-maximum cytoplasmic Na^+ concentration K_{dni} on C_o. $\Psi = 0$.

5 *B*. Experimentally, this effect appears as normalized I–V relations not changing significantly at $C_o \cong 16$ mM.

Effect of counterion concentration and membrane voltage on apparent cytoplasmic sodium affinity

The apparent affinities used in this paper are obtained from the ion-concentration dependence of exchange current. They are the reciprocals of the concentrations that correspond to half-maximal current. From Eq. 1, a half-maximum concentration of cytoplasmic sodium, K_{dni}, is obtained as

$$K_{dni} = \frac{K_{ni} Q^{1/3}}{1 - Q^{1/3}}, \tag{10}$$

where

$$Q = \frac{(a_2 + a_4 e^{\Psi/2}) f_{co}}{[a_3 + a_5 e^{\Psi/2} + 2(a_2 + a_4 e^{\Psi/2}) f_{co}] + a_6 e^{\Psi/2}}.$$

From Eq. 10, $K_{dni} \to 0$ as $C_o \to 0$. This is consistent with critical predictions of the consecutive Na^+–Ca^{2+} exchange model; that is, the half-maximal concentration for one ion species must vanish as the counterion concentration approaches zero (Lauger, 1987; Hilgemann, 1988). K_{dni} is an increasing function of C_o and saturates as C_o is increased. The calculated dependence of K_{dni} on C_o is presented in Fig. 6. It is noteworthy that this behavior, predicted from the eight-state model, is compatible with the detailed experimental data of Hilgemann et al. (1991). For example, the slope of K_{dni} versus C_o is given by (for simplicity, $\Psi = 0$)

$$\frac{dK_{dni}}{dC_o} = \frac{\omega_3 \omega_2^{1/3} K_{ni}}{3\left[1 - \left(\frac{\omega_2 C_o}{\omega_1 C_o + \omega_3}\right)^{1/3}\right]^2 [(\omega_1 C_o + \omega_3) C_o]^{2/3}}, \tag{11}$$

where $\omega_1 = a3 + a5 + a6 + 2\omega_2$, $\omega_2 = a_2 + a_4$, and $\omega_3 = a_6 K_{co}$, and is perpendicular (i.e., $dK_{dni}/dC_o \to \infty$) to the C_o axis at $C_o = 0$. Also, numerical solution demonstrates that the dependence of K_{dni} on C_o will be convex at any C_o, in agreement with experimental data.

The multistep consecutive models of Matsuoka and Hilgemann (1992), in agreement with experimental data, reveal a complex relationship between the maximum outward current I_{max} and K_{dni} as C_o is changed. The modeled I_{max} decreases more steeply than the modeled K_{dni}; that is, I_{max} decreases by 45% and K_{dni} by 24% as C_o is reduced from 2.0 to 0.35 mM. Here, we also show that the eight-state model does not predict a simple relationship between I_{max} and K_{dni}. From Eq. 11, $dK_{dni}/dC_o \propto C_o^{2/3}$ at small C_o. At the same time, $dI_{max}/dC_o \propto C_o^{-1}$; i.e. the dependence of $I_{max,N_i \to \infty}$ on C_o in the eight-state model is steeper at small C_o than that for K_{dni}.

Experimental studies of the voltage dependence of K_{dni} show some diversity. It has been estimated by Matsuoka and Hilgemann (1992) that K_{dni} decreases on depolarization from −100 mV to +100 mV at a constant C_o of 8 mM. A clear decrease of K_{dni} was not observed at strong hyperpolarization (~−125 mV). No significant shift of K_{dni} was obtained in a previous series of experiments (Hilgemann et al., 1991) as membrane potential was stepped from −80 to +20 mV. Our results may explain this diversity.

From Eq. 10, at very hyperpolarized levels (i.e., $\Psi \to -\infty$), K_{dni} approaches a constant value independently of C_o:

$$K_{dni,\Psi \to -\infty} = \frac{K_{ni} \eta^{1/3}}{1 - \eta^{1/3}}, \qquad \eta = \frac{3 l''_{ni}}{l'_{ni} + 6 l''_{ni}}.$$

$K_{dni,\Psi \to -\infty}$ is calculated to be 40 mM. From Eq. 10, a variation of K_{dni} with Ψ is given by

$$\frac{dK_{dni}}{d\Psi} = \frac{s_1 Q^{4/3} e^{\Psi/2}}{6 s_2 (1 - Q^{1/3})^2},$$

where $s_1 = f_{co} K_{ni}[(a_3 a_4 - a_2 a_5) f_{co} - a_2 a_6]$ and $s_2 = f_{co}(a_2 + a_4 e^{\Psi/2})$. The voltage dependence of K_{dni} is determined by the sign of s_1. If $s_1 < 0$, then $dK_{dni}/d\Psi < 0$, and K_{dni} is a decreasing function of Ψ and vice versa. Hence, a critical concentration of external Ca^{2+} that affects the voltage dependence of K_{dni} must exist. It can easily be shown from Eqs. 9 and 10 that this critical concentration coincides with

$\bar{C}_o$. At $C_o < \bar{C}_o$, $dK_{dni}/d\Psi > 0$, and K_{dni} is a decreasing function of Ψ and vice versa. At $C_o = \bar{C}_o$, K_{dni} does not depend on membrane voltage. Thus, the critical influence of C_o must be taken into account during experimentation. Calculated voltage dependencies of K_{dni} at different C_o are shown in Fig. 7.

"Forward zero-*trans*" conditions ($N_i = 0$, $C_o = 0$)

Current–voltage relations and maximum turnover rates

Equation A6 of the Appendix can be rewritten in terms of dependence on f_{ci}, f_{3no}, and Ψ:

$$I_i = -\frac{z_1 f_{ci} f_{3no}}{z_2 f_{3no} + z_3 f_{ci} f_{3no} + z_4 f_{ci} e^{\Psi} + z_5 f_{ci} e^{\Psi/2}}, \quad (12)$$

where z_1–z_5 are constants:

$$z_1 = e_o X k_{ci} k_{co} k_{ni} k_{no} l'_{ci} l'_{no} l''_{co} l''_{ni},$$

$$z_2 = 3(l''_{ci} + l''_{co}) k_{ci} k_{co} k_{ni} k_{no} l'_{no} l''_{ni},$$

$$z_3 = l'_{ci} l'_{no}\{k_{ni} l''_{co}[(k_{ci} k_{no} + 2k_{ci} l''_{ni} + 2k_{no} l''_{ni}) k_{co} + k_{ci} k_{no} l''_{ni}] + (k_{ni} + l''_{co}) k_{ci} k_{co} k_{no} l''_{ni}\},$$

$$z_4 = 3k_{ci} k_{co} k_{ni} k_{no} l'_{ci} l''_{co} l''_{no}, \qquad z_5 = 3k_{ci} k_{co} k_{ni} k_{no} l'_{ci} l''_{co} l''_{ni}.$$

Note that the condition of shielding of membrane voltage is not met in this case because the denominator contains a positive exponent, $e^{\Psi/2}$. I_i does not depend on C_i at $\Psi \geq 0$, if the following condition is met:

$$\frac{1}{f_{ci}} \ll \frac{L_{ci}}{3}\left(\frac{1}{k_{co}} + \frac{1}{k_{ni}} + \frac{1}{l''_{ni}} + \frac{1}{l''_{co}} + \frac{2}{k_{ci}} + \frac{2}{k_{no}} + \frac{3}{f_{3no} L_{no}}\right). \quad (13)$$

Analogously to outward current, the Ca_i-saturating concentration increases if N_o is increased, and from condition 13 it is calculated to be $\gg$0.1 μM at 50 mM N_o. This result is consistent with experiments (Matsuoka and Hilgemann, 1992) that reveal that, at N_o = 50 mM, I_i is completely saturated at 6 μM C_i. The dependence of inward I–V relations on C_i as calculated from Eq. 12 is shown in Fig. 8.

I_i does not depend on N_o if the following condition exists (at $\Psi \leq 0$):

$$\frac{1}{f_{3no}} \ll \frac{L_{no}}{3}\left(\frac{1}{k_{co}} + \frac{1}{k_{ni}} + \frac{1}{l''_{ni}} + \frac{1}{l''_{co}} + \frac{2}{k_{ci}} + \frac{2}{k_{no}} + \frac{3}{f_{ci} L_{ci}}\right). \quad (14)$$

Na_o-saturation concentration increases if C_i concentration is increased, and it is calculated to be $\gg$230 mM at 5 μM C_i and $\gg$340 mM at 0.1 mM C_i. This calculation cannot easily be tested under experimental conditions.

I_i is an increasing function of Ψ and asymptotically approaches zero at highly depolarized potentials (i.e., as $\Psi \to \infty$). Under strong hyperpolarization (i.e., as $\Psi \to -\infty$), I_i saturates and approaches the minimum negative value of exchange current:

$$I_{\min,\Psi\to-\infty} = -\frac{z_1 f_{ci}}{z_2 + z_3 f_{ci}}. \quad (15)$$

Note that $I_{\min,\Psi\to-\infty}$ does not depend on N_o, in agreement with experimental findings (Hilgemann et al., 1991). Equation 15 reveals that $I_{\min,\Psi\to-\infty}$ practically does not depend on C if $z_3 f_{ci} \gg z_2$. In terms of rate constants, this condition is obtained as

$$\frac{1}{f_{ci}} \ll \frac{L_{ci}}{3}\left(\frac{1}{k_{co}} + \frac{1}{k_{ni}} + \frac{1}{l''_{ni}} + \frac{1}{l''_{co}} + \frac{2}{k_{ci}} + \frac{2}{k_{no}}\right). \quad (16)$$

The Ca_i saturation concentration corresponding to condition 16 is calculated to be $\gg$90 μM.

From Eq. A8 below, the maximum inward turnover rate $\nu_{i,max}$ can be defined as $\Psi \to -\infty$ and the infinite concentration of transported Ca^{2+} (i.e., $f_{ci} = 1$):

$$\nu_{i,max} = \left(\frac{1}{k_{co}} + \frac{1}{k_{ni}} + \frac{1}{l''_{co}} + \frac{1}{l''_{ni}} + \frac{2}{k_{ci}} + \frac{2}{k_{no}} + \frac{3}{L_{ci}}\right)^{-1}.$$

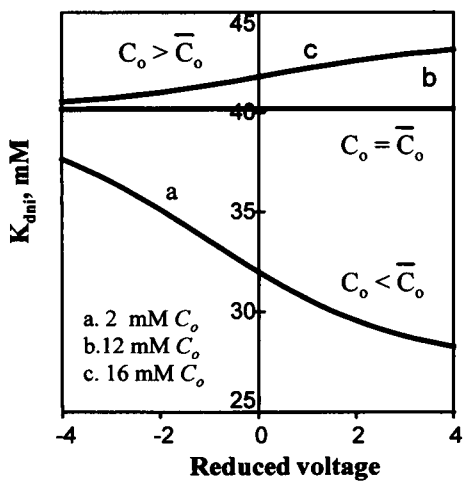

FIGURE 7 Voltage dependence of K_{dni} at different values of C_o.

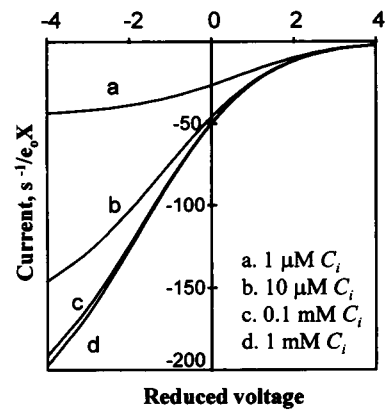

FIGURE 8 Dependence of inward I–V relations on C_i at N_o = 150 mM.

With the above values of rate constants, one finds that $\nu_i \cong 260\ s^{-1}$. A maximum inward turnover rate under short-circuit conditions (i.e., $\Psi = 0$) is given by

$$\nu_{i.s.c} = \left(\frac{1}{k_{co}} + \frac{1}{k_{ni}} + \frac{1}{l''_{co}} + \frac{1}{l''_{ni}} + \frac{2}{k_{ci}} + \frac{2}{k_{no}} + \frac{3}{L_{ci}} + \frac{3}{L_{no}}\right)^{-1}.$$

$\nu_{i.s.c}$ is calculated to be $\sim 220\ s^{-1}$, i.e., almost the same as that at infinite hyperpolarization, in contrast to "reverse zero-*trans*" conditions.

The absolute value of I_i increases as C_i is increased, and I_{max} as $C_i \to \infty$ is given by

$$|I_{max,\,C_i\to\infty}| = \frac{z_1 f_{3no}}{r_1 + r_2 f_{3no}}, \tag{17}$$

where $r_1 = z_4 e^{\Psi} + z_5 e^{\Psi/2}$ and $r_2 = z_2 + z_3$. Note that $I_{max,C_i\to\infty}$ depends on membrane voltage. The absolute value of $I_{max,C_i\to\infty}$ decreases as N_o is decreased, consistent with the Ca_i-saturation concentration being decreased as N_o is reduced (Matsuoka and Hilgemann, 1992). $I_{max,C_i\to\infty}$ will not depend on N_o if condition 14, with the substitution $f_{ci} = 1$, holds. The Na_o-saturation concentration is reduced with hyperpolarization but is still moderately high: $N_o \gg 116$ mM at $\Psi = -3$, and $N_o \gg 90$ mM at $\Psi = -4$.

Effect of ion concentration on the shape of inward I–V relations

Experimental data for inward exchange current (Hilgemann et al., 1991; Matsuoka and Hilgemann, 1992) reveal that the shape of inward I–V relations depends on both N_o and C_i. There was some flattening of the I–V relations at low C_i and at high N_o, and slopes depended only slightly on C_i.

The slope of inward I–V relations is given by

$$\frac{dI_i}{d\Psi} = \frac{z_1(2z_4 e^{\Psi} + z_5 e^{\Psi/2}) f_{ci}^2 f_{3no}}{2[(z_4 e^{\Psi} + z_5 e^{\Psi/2}) f_{ci} + (z_2 + z_3 f_{ci}) f_{3no}]^2}. \tag{18}$$

Although the slope of I–V relations is an increasing function of C_i (Fig. 9), it can be seen from Eq. 18 that the slope will not depend on C_i at $\Psi \geq 0$ if condition 13 is met. The result corresponds to experimental data (Matsuoka and Hilgemann, 1992) that reveal that the slope of I–V relations does not change at $C_i > 64\ \mu M$.

Fig. 9 displays a complex relation between the slope of inward I–V curves and N_o: slopes are less at low C_i as N_o is elevated from 150 to 300 mM. Equation 18 shows that $dI_i/d\Psi$ is a decreasing function of N_o, expressed through f_{3no}, if $f_{3no} > \bar{f}_{3no}$, and vice versa. Here, $\bar{f}_{3no}$ is a critical fraction of exchanger occupied by external Na^+. $\bar{f}_{3no}$ and the critical external Na^+ concentration $\bar{N}_o$ are given by, respectively,

$$\frac{1}{\bar{f}_{3no}} = \frac{L_{no}}{3}\left(\frac{1}{k_{co}} + \frac{1}{k_{ni}} + \frac{1}{l''_{ni}} + \frac{1}{l''_{co}} + \frac{2}{k_{ci}} + \frac{2}{k_{no}} + \frac{3}{f_{ci}L_{ci}}\right), \tag{19}$$

$$\bar{N}_o = \frac{K_{no}\bar{f}_{3no}^{1/3}}{1 - \bar{f}_{3no}^{1/3}}.$$

The calculated dependence of the slope of I–V relations on N_o at different C_i and $\Psi = 0$ is presented in Fig. 10. It can be seen that $\bar{N}_o$ increases as C_i is increased, and from Eqs. 19 it is calculated to be ~ 130 mM at 1 μM, ~ 230 mM at 5 μM, and ~ 340 mM at 0.1 mM C_i. Comparable experimental data are not available.

The concavity of inward I–V relations depends on membrane potential, N_o and C_i. The function will be concave at $l''_{ni} \cong l''_{no}$, if the following relation holds:

$$(z_2 + z_3 f_{ci})(1 + 4e^{\Psi/2}) > \frac{z_4 f_{ci}}{f_{3no}}[3e^{\Psi/2} + (1 + 4e^{\Psi})]e^{\Psi/2}. \tag{20}$$

Generally, it can be seen that I–V relations will be convex at very depolarized levels (i.e., $\Psi \to \infty$) and concave at high hyperpolarization (i.e., $\Psi \to -\infty$), consistent with current saturation at those potentials. A decreasing C_i and an increasing N_o will favor the function becoming concave, which is consistent with experimental data in the range ± 50

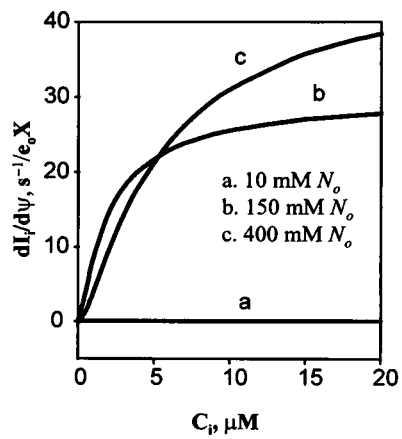

FIGURE 9 Dependence of the slope of inward I–V relations on C_i at different values of N_o. $\Psi = 0$.

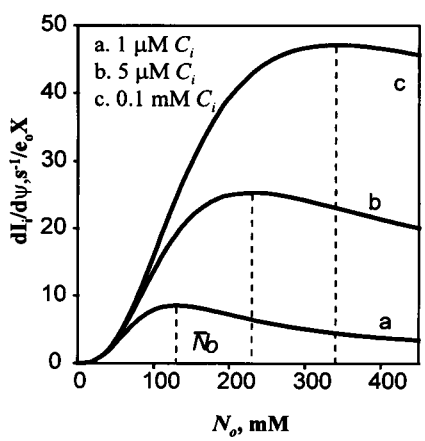

FIGURE 10 Dependence of the slope of inward I–V relations on N_o at different values of C_i. $\Psi = 0$.

mV, where the I–V relation is convex at 100 mM N_o and is concave with 400 mM N_o (Hilgemann et al., 1991). The dependence of inward I–V relations on N_o calculated according to Eq. 12 is presented in Fig. 11. The potential of I–V inflection can be found from relation 20 transformed into the equation. In accordance with Ca_i saturation, the potential of inflection does not depend on C_i, provided that condition 16 holds.

Effect of counterion concentration and membrane voltage on apparent cytoplasmic calcium affinity

An expression for the dependence of half-maximum cytoplasmic Ca^{2+} concentration K_{dci} on external Na^+ concentration can be derived from Eqs. 12 and 17:

$$K_{dci} = \frac{K_{ci} z_2 f_{3no}}{r_1 + r_2 f_{3no}}. \tag{21}$$

As can be seen, K_{dci} is independent of N_o if condition 14 is held. Equation 21 shows that $K_{dci} = 0$ at $N_o = 0$. This result is similar to that for K_{dni} and is also consistent with critical predictions from the consecutive model. However, the dependence of K_{dci} on N_o has some peculiarities. The derivative of K_{dci} with respect to N_o is given by (for simplicity, $\Psi = 0$)

$$\frac{dK_{dci}}{dN_o} = \frac{3\theta_2\theta_3 K_{no}(N_o + K_{no})^2 N_o^2}{\{\theta_1 N_o^3 + \theta_2 K_{no}[K_{no}^2 + 3(N_o + K_{no})N_o]\}^2}, \tag{22}$$

where $\theta_1 = r_2 + z_4 + z_5$, $\theta_2 = z_4 + z_5$, and $\theta_3 = z_2 K_{ci}$. K_{dci} is an increasing, saturable function of N_o. As $N_o \to 0$, $dK_{dci}/dN_o = 0$; i.e., the function is parallel to the N_o axis at $N_o \cong 0$. The graph of the function can be concave or convex, depending on N_o (convex at high N_o). The dependence of K_{dci} on N_o as calculated from Eq. 21 is presented in Fig. 12. The point of inflection is numerically calculated to be ≅100 mM, compatible with experimental data of Hilgemann et al. (1991).

The variation of K_{dci} with membrane potential is given by

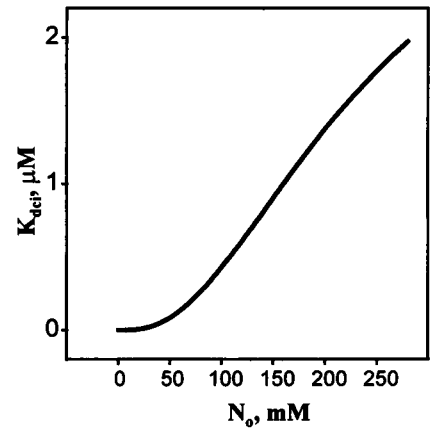

FIGURE 12 Dependence of half-maximum cytoplasmic Ca^{2+} concentration K_{dci} on N_o. $\Psi = 0$.

$$\frac{dK_{dci}}{d\Psi} = -\frac{z_2 K_{ci} f_{3no}(1/2 z_5 + z_4 e^{\Psi/2}) e^{\Psi/2}}{(r_1 + r_2 f_{3no})^2}. \tag{23}$$

Two important features can be seen from Eq. 23. First, K_{dci} is a decreasing function of membrane potential at every Ψ, and second, the dependence of $dK_{dci}/d\Psi$ on N_o is steeper as N_o is reduced, consistent with voltage dependence of the rate-limiting step. Calculated dependencies of K_{dci} on membrane voltage at different N_o are presented in Fig. 13. The results are consistent with experimental data showing that the apparent K_{dci} increases, on average, 89 ± 3% with stimulation of the current by hyperpolarization from +20 to −80 mV (Hilgemann et al., 1991).

DISCUSSION AND CONCLUSIONS

Theoretical analysis of the eight-state consecutive model and the simulation procedure show that the mathematically obtained characteristics of the Na^+–Ca^{2+} exchange cycle are consistent with experimental results. Identified critical points and predictions can now be used for further comprehensive experimental tests of the model.

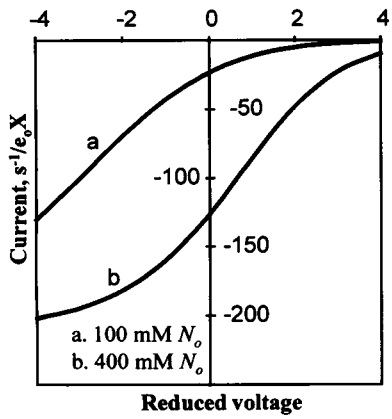

FIGURE 11 Dependence of inward I–V relations on N_o at C_i = 20 μM.

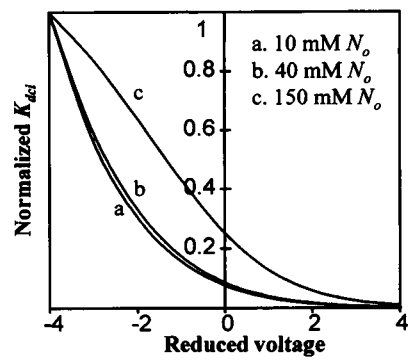

FIGURE 13 Voltage dependence of K_{dci} at different values of N_o. Values were normalized to K_{dci} at $\Psi = -4$.

We have identified a number of conditions that determine the probability of transferring the Na^+–Ca^{2+} exchange cycle to a specific state that is either saturated or exhausted with respect to the transported ions. The majority of these states depend on the counterion concentration. Thus, the role of the counterion should be taken into account during design of experiments and data interpretation. It is of interest that, for outward current, some threshold Na^+ and Ca^{2+} concentrations were found. For example, the Ca_o-exhaustion state cannot be reached if C_o exceeds a certain value (1.2 mM in simulation). Similarly, the Na_i-saturation state cannot be attained if N_i is below a certain value (500 mM in simulation). These critical concentrations may serve specific roles in cellular metabolism.

The calculation of maximum turnover rate, disregarding exchanger site density, is another important feature of this study. Most previous calculations were done on the basis of estimated exchanger density and revealed a rapid turnover rate for the exchanger protein. A turnover rate of $\sim$1000 s^{-1} was found in reconstituted proteoliposomes by Cheon and Reeves (1988). Niggli and Lederer (1991) suggested $\sim$250 exchangers/μm^2 and indicated an upper estimate of $\sim$2,500 s^{-1} for the turnover rate. Charge movement experiments (Hilgemann et al., 1991) determined $\sim$400 exchangers/μm^2 and maximum turnover rates of 5,000 s^{-1}. In contrast, Powell et al. (1993), on the basis of current relaxation studies in response to cytoplasmic Ca^{2+} jumps, estimated that the inward turnover rate at -80 mV and 36°C is <300 s^{-1}, consistent with our estimates based on numerical values of rate constants. Turnover rates of $\sim$50 s^{-1} were found for the purified Na^+–Ca^{2+}, K^+ exchanger from rod outer segments (Cook and Kaupp, 1988; Nicoll and Applebury, 1989), although this protein is both functionally and structurally distinct from cardiac Na^+–Ca^{2+} exchangers. Here, we find that the turnover rate cannot be described in terms of a single rate constant but depends on a combination of rate constants belonging to the exchange cycle. Turnover rate is a function of membrane voltage and the concentrations of transported ions and can be different for inward and outward exchange modes. Interestingly, the inward turnover rate, in contrast to the outward, does not show a strong dependence on membrane voltage. Thus, during an action potential, changes in turnover rate may be controlled more by ion concentration changes than by membrane voltage.

Identified interconnections between the factors that control the Na^+–Ca^{2+} exchange cycle (i.e., Na^+ and Ca^{2+} concentrations, membrane potential) appear as changes of apparent ion affinities and shape changes of the outward and inward I–V relations. A complete loss of voltage dependence can be observed as ion concentrations are manipulated. Basically, all these changes depend on the relationships between the rates of voltage-dependent Na^+ transport and nonelectrogenic (electrically silent) Ca^{2+} translocation. Alterations in the flux rates cause alterations in the electrical portrait of the Na^+–Ca^{2+} exchange cycle. Therefore, introduction of a criterion for evaluating the contribution of each flux would be useful for interpretation of experimentally obtained and simulated results.

It can be seen from Eq. 5 that, in the case when $\Psi \to \infty$ and $f_{co} \to 1$, I_o approaches the limiting value:

$$I_{max,\Psi\to\infty}^{C_o\to\infty} = \frac{a_1 f_{3ni}}{a_4+(a_5+a_6)f_{3ni}}.$$

The difference between $I_{max,\Psi\to\infty}^{C_o\to\infty}$ and $I_{max,\Psi\to\infty}$ is the nonelectrogenic part of I_o under diffusion control by electrically silent Ca^{2+} influx. Therefore, a factor ε_o is introduced here as a measure of the influence of membrane potential on the Na^+–Ca^{2+} exchange transport processes. ε_o can be defined as the fraction of maximum outward exchange current that is governed by membrane potential and is given as

$$\varepsilon_o = \frac{I_{max,\Psi\to\infty}}{I_{max,\Psi\to\infty}^{C_o\to\infty}} = \frac{[a_4+(a_5+a_6)f_{3ni}]f_{co}}{a_6 f_{3ni}+(a_4+a_5 f_{3ni})f_{co}}. \quad (24)$$

From Eq. 24, as $C_o \to \infty$ and $f_{co} \to 1$, $\varepsilon_o \to 1$; in other words, the exchange cycle is driven completely by membrane voltage (voltage control), consistent with voltage-dependent Na^+ efflux being rate limiting. In contrast, as $C_o \to 0$ and $f_{co} \to 0$, $\varepsilon_o \to 0$, i.e.; in this case the exchange cycle is completely governed by electrically silent Ca^{2+} influx (diffusion control). ε_o depends on cytoplasmic Na^+ concentration. As $N_i \to 0$ and $f_{3ni} \to 0$, $\varepsilon_o \to 1$, consistent with voltage-dependent Na^+ efflux being rate limiting. It is of interest that, as $N_i \to \infty$ and $f_{3ni} \to 1$, $\varepsilon_o \neq 0$; that is, the outward exchange cycle does not come under complete diffusion control, as Na^+ efflux dominates the process. Apparently, this reflects the fact that Na^+ efflux contains both diffusion and kinetic (voltage-dependent) components. In this case ε_o is given by

$$\varepsilon_{o,N_i\to\infty} = \frac{(a_4+a_5+a_6)f_{co}}{a_6+(a_4+a_5)f_{co}}.$$

This limiting value of ε_o is calculated to be 0.69 at 8 mM C_o. The dependence of ε_o on C_o at different values of N_i is presented in Fig. 14.

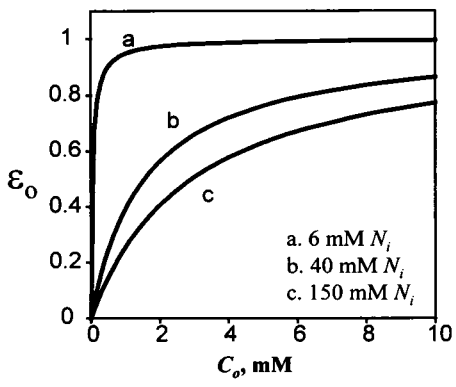

FIGURE 14 Dependence of ε_o on C_o at different values of N_i.

ε_o can be conveniently used for the interpretation of theoretical and experimental results. For example, the experimentally determined loss of voltage dependence of I_o when $C_o < 0.2$ mM (Matsuoka and Hilgemann, 1992) corresponds to $\varepsilon_o < 0.07$ (with $\varepsilon_{o,N_i \to \infty} = 0.05$). Theoretically defined conditions of Ca^{2+} exhaustion (i.e., Eqs. 3 and 4) reveal that complete loss of voltage dependence will take place at $\varepsilon_o \ll 0.5$. These conditions can be realized only at $C_o < 1.2$ mM, (i.e., at $\varepsilon_o < 0.26$). Similarly, theoretically and experimentally determined Ca^{2+}-saturation conditions correspond to $\varepsilon_o \gg 0.5$. In light of these values, the biphasic behavior of outward I–V relation slopes (Fig. 4) can easily be explained. The dependence of ε_o on N_i at different values of C_o, corresponding to the conditions illustrated in Fig. 4, is presented in Fig. 15. At low N_i (i.e., primarily a voltage-controlled exchange cycle), voltage-dependent Na^+ transport is rate limiting, and its rate increases as N_i is increased. When ε_o approaches a certain value (i.e., $\varepsilon_o \leq 0.26$ for both 0.2 and 0.5 mM C_o) that reflects the rate-limiting character of electrically silent Ca^{2+} transport, the exchange cycle becomes more diffusion controlled, and the slope of I–V relations decreases as N_i is increased. An ε_o value of 0.26 can never be attained at $C_o > 1.2$ mM. Therefore, the slope increases monotonically as N_i is increased in the presence of 2 mM C_o. This means that, above a certain C_o, Ca^{2+} influx cannot be rate limiting at any N_i under reverse "zero-*trans*" conditions.

ε_o is calculated to be 0.3 and 0.9 for 100 and 8 mM N_i (C_o in both cases is 1 mM), respectively. Therefore, outward current gains in steepness as N_i is reduced, as can be seen from Fig. 5 and experimental data from Matsuoka and Hilgemann (1992) and Doering et al. (1996).

Because Eq. 15 for $I_{i,\Psi \to -\infty}$ does not contain N_o, Eq. 12 for I_i at $\Psi = 0$ can be used for evaluation of a factor, ε_i, that is the counterpart to ε_o. If $C_i \to \infty$ and $f_{ci} \to 1$, then the inward exchange current approaches the limiting value

$$|I_{\Psi=0}^{C_i \to \infty}| = \frac{z_1 f_{3no}}{z_4 + z_5 + (z_2 + z_3) f_{3no}}.$$

The difference between $|I_{\Psi=0}^{C_i \to \infty}|$ and $|I_{\Psi=0}|$ reflects a nonelectrogenic component of I_i that is under diffusion control by electrically silent Ca^{2+} efflux. Therefore, ε_i can serve as a measure of voltage control of the inward exchange cycle and is defined as

$$\varepsilon_i = \frac{|I_{\Psi=0}|}{|I_{\Psi=0}^{C_i \to \infty}|} = \frac{[z_4 + z_5 + (z_2 + z_3) f_{3no}] f_{ci}}{(z_2 + z_3 f_{ci}) f_{3no} + (z_4 + z_5) f_{ci}}. \quad (25)$$

From Eq. 25, as $C_i \to \infty$ and $f_{ci} \to 1$, $\varepsilon_i \to 1$, the exchange cycle is completely governed by membrane voltage, consistent with voltage-dependent Na^+ influx being rate limiting. In contrast, as $C_i \to 0$ and $f_{ci} \to 0$, $\varepsilon_i \to 0$, the exchange cycle is completely driven by electrically silent Ca^{2+} efflux. As $N_o \to 0$ and $f_{3no} \to 0$, $\varepsilon_i \to 1$, consistent with voltage-dependent Na^+ influx being rate limiting. Here ε_i attains the limiting value

$$\varepsilon_{i,N_o \to \infty} = \frac{(z_2 + z_3 + z_4 + z_5) f_{ci}}{z_2 + (z_3 + z_4 + z_5) f_{ci}}.$$

The calculated dependence of ε_i on C_i at different N_o is presented in Fig. 16. It can be seen that the inward exchange cycle is primarily voltage controlled under typical experimental conditions (e.g., $\varepsilon_i > 0.5$ above 2.2 μM C_i in the presence of 300 mM N_o) because of a very high cytoplasmic Ca^{2+} affinity.

Application of ε_i for interpretation of theoretical and experimental results shows that the above-mentioned conditions of Ca_i saturation (i.e., independence of I_i, slope and inflection potential of inward I–V relations on C_i) are realized if $\varepsilon_i \gg 0.54$. I_i and K_{dci} independence of N_o occurs when $\varepsilon_i \gg 0.61$.

Biphasic behavior of the slope of inward I–V relations in response to changes in N_o (Fig. 10) reflects the different voltage dependences of the rate-limiting steps. At low N_o the voltage-dependent Na^+ occlusion reaction on the extracellular side could be rate limiting. This rate sharply increases as N_o is increased until the electrically silent Ca^{2+} transport becomes rate limiting. Apparently the rates of Na^+ and Ca^{2+} transport are equal at $\bar{N}_o$. It is of interest that the inward exchange cycle remains under voltage control,

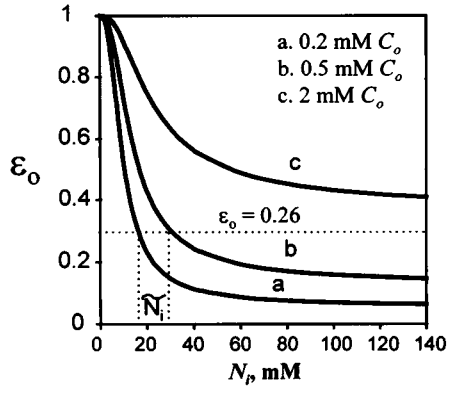

FIGURE 15 Dependence of ε_o on N_i at different values of C_o.

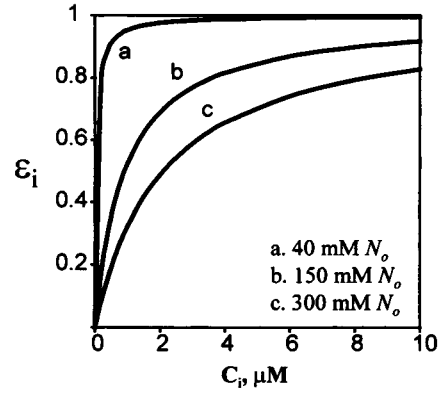

FIGURE 16 Dependence of ε_i on C_i at different values of N_o.

whereas the Ca^{2+} efflux becomes rate limiting. The maximum points indicated in Fig. 10 correspond to the following values of ε_i: (*a*) 0.59, (*b*) 0.76, and (*c*) 0.97.

As N_o is reduced, ε_i increases. Therefore, outward current gains in steepness as N_o is reduced, as shown in Fig. 11 and the experimental data of Hilgemann et al. (1991). The same explanation can be applied to account for the influence of N_o on the voltage dependence of K_{dci} (Fig. 13).

In conclusion, the general solution obtained for the eight-state consecutive model can be used conveniently for a comprehensive analysis of the Na^+–Ca^{2+} exchange mechanism. Predictions from this model are in accord with most experimental data. In addition, a variety of behaviors is predicted that can now be employed to test further the fidelity of this model. Finally, this analytical solution can be used to assess other similar transport mechanisms by simple assignment of appropriate rate constants.

APPENDIX

General solution for Na^+–Ca^{2+} exchange current

The expression for exchange current was obtained with LAMKIN computer software adapted from the program published by Lam (1981). The program is based on the diagram method of King and Altman (1956). The expanded mathematical expressions were simplified by use of a symbolic algebraic language (Theorist; Waterloo Maple Software) to yield a readable final result. This result was checked thoroughly with Theorist to match the expanded form of the original solution.

For a system containing X exchanger molecules per unit of membrane area, the outward exchange current, corresponding to net Ca^{2+} influx, is given by the general equation

$$I = e_o X(Y_i - Y_o)/Z, \tag{A1}$$

where e_o is the elementary electric charge, Y_i and Y_o are the products of 8 rate constants derived from flux diagrams corresponding to inward and outward Ca^{2+} fluxes, respectively, and Z is the sum of 64 directional diagrams for all states. Intermediate variables p_1–p_8, are given by

$$p_1 = (k_{87} + k_{81})[(k_{43} + k_{34})k_{65}k_{54} + (k_{65} + k_{56})k_{45}k_{34}]k_{76}k_{23}k_{12},$$

$$p_2 = (k_{67} + k_{65})[(k_{21} + k_{12})k_{43}k_{32} + (k_{43} + k_{34})k_{23}k_{12}]k_{81}k_{78}k_{54},$$

$$p_3 = (k_{23} + k_{21})[(k_{65} + k_{56})k_{87}k_{76} + (k_{87} + k_{78})k_{67}k_{56}]k_{45}k_{34}k_{18},$$

$$p_4 = (k_{45} + k_{43})[(k_{21} + k_{12})k_{81}k_{78} + (k_{87} + k_{78})k_{21}k_{18}]k_{67}k_{56}k_{32},$$

$$p_5 = \{[(k_{87} + k_{81})k_{76}k_{43} + (k_{76} + k_{43})k_{87}k_{18}]k_{54} + [(k_{45} + k_{43})k_{87}k_{76} + (k_{78} + k_{76})k_{54}k_{43}]k_{18}\}k_{65}k_{32}k_{21},$$

$$p_6 = \{\{[(k_{32} + k_{23})k_{65} + (k_{65} + k_{32})k_{21}]k_{87}k_{76} + (k_{87} + k_{78})k_{67}k_{32}k_{21}\}k_{18} + (k_{87} + k_{81})k_{76}k_{65}k_{32}k_{12}\}k_{54}k_{43},$$

$$p_7 = \{[(k_{45} + k_{43})k_{56} + (k_{56} + k_{45})k_{34}]k_{81}k_{78}k_{67} + [(k_{81} + k_{67})k_{78} + (k_{87} + k_{81})k_{67}]k_{56}k_{45}k_{34}\}k_{23}k_{12},$$

$$p_8 = [(k_{23} + k_{21} + k_{12})k_{67}k_{56} + k_{65}k_{23}k_{12}]k_{81}k_{78}k_{45}k_{34} + [(k_{23} + k_{21})k_{65}k_{54}k_{34} + (k_{45} + k_{43})k_{56}k_{32}k_{21}]k_{87}k_{76}k_{18}.$$

The general solutions for Y_i, Y_o, and Z are

$$Y_i - Y_o = k_{81}k_{78}k_{67}k_{56}k_{45}k_{34}k_{23}k_{12} - k_{87}k_{76}k_{65}k_{18}k_{54}k_{43}k_{32}k_{21},$$

$$Z = p_1 + p_2 + \cdots + p_8.$$

Assignment of rate constants and numerical values used in simulation

Numerical values of rate and binding constants for Na^+–Ca^{2+} exchange were selected from the literature (Blaustein, 1977; Requena, 1978; DiPolo, 1979; Baker and DiPolo, 1984; Johnson and Kootsey, 1985; Johnson et al., 1992; Allen and Baker, 1986; Lauger, 1987; Hilgemann, 1988; Hilgemann et al., 1991; Matsuoka and Hilgemann, 1992) on the basis of certain principles and assumptions noted below. Some of the parameters were modified slightly to correspond more closely to existing experimental data.

With the fractions of exchanger molecules in state j designated f_j, the binding reactions on the cytoplasmic side are described by equilibrium dissociation constants K_{1ni}, K_{2ni}, and K_{3ni} for binding of the first, second, and third cytoplasmic Na^+, respectively, and K_{ci} for binding cytoplasmic Ca^{2+}:

$$K_{1ni} = \frac{f_{oi}}{f_{1ni}} N_i, \qquad K_{2ni} = \frac{f_{1ni}}{f_{2ni}} N_i,$$

$$K_{3ni} = \frac{f_{2ni}}{f_{3ni}} N_i, \qquad K_{ci} = \frac{f_{oi}}{f_{ci}} C_i.$$

Analogous equations hold for the extracellular side:

$$K_{1no} = \frac{f_{oo}}{f_{1no}} N_o, \qquad K_{2no} = \frac{f_{1no}}{f_{2no}} N_o,$$

$$K_{3no} = \frac{f_{2no}}{f_{3no}} N_o, \qquad K_{co} = \frac{f_{oo}}{f_{co}} C_o.$$

Here, f_{oi} and f_{oo} represent the fractions of unloaded exchanger molecules on the cytoplasmic and extracellular sides, respectively. N_i and C_i represent the concentrations of Na^+ and Ca^{2+} in the cytoplasm, respectively, and N_o and C_o are their extracellular counterparts.

Because of the voltage independence and equilibria of the binding reactions, the microscopic reversibility enforced on the dissociation constants is given as

$$\frac{K_{ci}K_{1no}K_{2no}K_{3no}}{K_{co}K_{1ni}K_{2ni}K_{3ni}} = 1. \tag{A2}$$

The fractions of exchanger molecules with 3 Na^+ bound intracellularly and those with Ca^{2+} bound on the cytoplasmic side are given by

$$f_{3ni} = \left(\frac{N_i^3}{K_{1ni}K_{2ni}K_{3ni}}\right)\Big/ D_i, \qquad f_{ci} = (C_i/K_{ci})/D_i.$$

The denominator D_i is defined as follows:

$$D_i = 1 + \frac{N_i}{K_{1ni}} + \frac{N_i^2}{K_{1ni}K_{2ni}} + \frac{N_i^3}{K_{1ni}K_{2ni}K_{3ni}} + \frac{C_i}{K_{ci}}.$$

Similarly, for the extracellular side, the following expressions can be

written:

$$f_{3no} = \left(\frac{N_o^3}{K_{1no}K_{2no}K_{3no}}\right)\Big/ D_o, \qquad f_{co} = (C_o/K_{co})/D_o,$$

where

$$D_o = 1 + \frac{N_o}{K_{1no}} + \frac{N_o^2}{K_{1no}K_{2no}} + \frac{N_o^3}{K_{1no}K_{2no}K_{3no}} + \frac{C_o}{K_{co}}.$$

Assuming that all Na^+-binding sites are independent, we employ the statistical expressions typically used to describe the relations between dissociation constants in an equilibrium system with multiple binding sites (Tanford, 1961; Lauger, 1987):

$$K_{1ni} = \frac{1}{3}K_{ni}, \qquad K_{2ni} = K_{ni}, \qquad K_{3ni} = 3K_{ni},$$

$$K_{1no} = \frac{1}{3}K_{no}, \qquad K_{2no} = K_{no}, \qquad K_{3no} = 3K_{no} \tag{A3}$$

In squid giant axons the experimentally defined value of the dissociation constant for Na^+ on the cytoplasmic side ranges from 34 to 50 mM (Blaustein, 1977; Requena, 1978; DiPolo, 1979), and that from the fitting procedure (Hilgemann et al., 1991; Matsuoka and Hilgemann, 1992), recalculated here as $K_{ni} = (K_{1ni}K_{2ni}K_{3ni})^{1/3}$, ranges from 16 to 29 mM. The designated value of K_{ni} used in our simulation was selected to be 30 mM. Experimentally determined and fitted results indicate that the binding affinity of Ca^{2+} is strongly asymmetric: the half-saturating concentration for external Ca^{2+} is 100–1000 times greater than that for cytoplasmic Ca^{2+} (Requena, 1978; Baker and DiPolo, 1984; Allen and Baker, 1986; Hilgemann et al., 1991; Matsuoka and Hilgemann, 1992). The designated concentration values used in our simulation were 10 μM and 10 mM for internal and external Ca^{2+}, respectively. K_{no} was calculated from Eqs. A2 and A3.

Because all binding reactions are treated as instantaneous equilibria, we can write the following equations for the association and dissociation rates for the Na^+ and Ca^{2+} transport complexes on the cytoplasmic and extracellular sides, respectively:

$$k_{12} = k_{21} = k_{ni} = K_{ni}\kappa_n, \qquad k_{54} = k_{45} = k_{no} = K_{no}\kappa_n,$$

$$k_{18} = k_{81} = k_{ci} = K_{ci}\kappa_c, \qquad k_{56} = k_{65} = k_{co} = K_{co}\kappa_c,$$

where κ_n and κ_c are the corresponding intrinsic association rate constants (expressed in $M^{-1}\ s^{-1}$) for Na^+ and Ca^{2+}, respectively.

Assuming that ion-binding reactions are diffusion limited, the intrinsic association rate constants on both the cytoplasmic and the extracellular sides were chosen to be 1×10^8 and $4 \times 10^8\ M^{-1}\ s^{-1}$ for Na^+ and Ca^{2+} binding, respectively. A maximum possible diffusion-limited complexation rate in aqueous solution is $5 \times 10^8\ M^{-1}\ s^{-1}$ (Diebler et al., 1969).

In the framework of this model, only those fractions of exchanger that have bound 3 Na^+ (or bound 1 Ca^{2+}) will undergo translocation. Thus, the rate of the Na^+ occlusion reaction on the cytoplasmic side, k_{23}, should be proportional to the fraction of exchangers loaded with 3 Na^+ ions:

$$k_{23} = l'_{ni}f_{3ni}. \tag{A4}$$

With electrogenicity occurring exclusively with occlusion–deocclusion of Na^+ on the extracellular side, the occlusion rate on the extracellular side, k_{43}, should include a dependence on membrane potential, E_m:

$$k_{43} = l'_{no}f_{3no}e^{-\Psi/2} \tag{A5}$$

where Ψ is the reduced voltage, $\Psi = E_m/(kT/e_o)$. The value of $kT/e_o \approx 25$ mV, and l'_{ni} and l'_{no} in Eqs. A4 and A5 are the corresponding intrinsic occlusion rate constants.

The rates of Na^+ deocclusion reactions on the cytoplasmic and extracellular sides are, respectively,

$$k_{32} = l''_{ni}, \qquad k_{34} = l''_{no}e^{\Psi/2},$$

where l''_{ni} and l''_{no} are intrinsic deocclusion rate constants.

Assuming that the Ca^{2+} translocation is voltage independent (i.e., electrically silent), the rates of the Ca^{2+} occlusion reactions are given by

$$k_{67} = l'_{co}f_{co}, \qquad k_{87} = l'_{ci}f_{ci},$$

where l'_{co} and l'_{ci} are the intrinsic Ca^{2+} occlusion rate constants for the extracellular and the cytoplasmic sides, respectively. The rates of the Ca^{2+} deocclusion reactions on the extracellular and the cytoplasmic sides are, respectively, as follows:

$$k_{76} = l''_{co}, \qquad k_{78} = l''_{ci}.$$

Limited data are available regarding transition rate constants. Lauger (1987) suggested that "at least one of the rate constants must be of the order of 100 s^{-1} or less." Experimentally estimated ion deocclusion rates for the Na, K pump lie in the range 0.001–100 s^{-1} (Forbush, 1988). The upper limit of $10^5\ s^{-1}$ was assumed by Johnson and Kootsey (1985), and the fitting procedure (Hilgemann et al., 1991) leads to values in the range 10^4–$5.2 \times 10^4\ s^{-1}$. With respect to the nearly symmetrical effects of cytoplasmic and extracellular Na^+, we suggest that $l'_{ni} = l'_{no} = 10^4\ s^{-1}$ and that $l''_{ni} = l''_{no} = 10^3\ s^{-1}$. Asymmetric effects of cytoplasmic and extracellular Ca^{2+} reflect a large difference in Ca^{2+} binding affinities between the cytoplasmic and extracellular sides (i.e., the Ca^{2+} binding "ion well" is deeper on the cytoplasmic side). Assuming equal occlusion rates for Ca^{2+} on both sides (i.e., $l'_{ci} = l'_{co} = 10^4\ s^{-1}$), the condition $l'_{ci} > l'_{co}$ has to be fulfilled. At $l''_{ci} = 10^4\ s^{-1}$ the value of $l''_{co} = 2 \times 10^3\ s^{-1}$ matches most existing experimental data.

Outward and inward current–voltage relations

The I–V relation for both outward and inward Na^+–Ca^{2+} exchange currents is provided by

$$I = e_o X \nu, \tag{A6}$$

where ν is the corresponding turnover rate. The expression for the outward turnover rate ν_o reads as

$$\nu_o = \left(\frac{1}{k_{ci}} + \frac{1}{k_{no}} + \frac{1}{l''_{ci}} + \frac{1}{l''_{no}e^{\Psi/2}} + \frac{2}{k_{co}} + \frac{2}{k_{ni}} + \frac{3}{f_{co}L_{co}} + \frac{3}{f_{3ni}L_{ni}}\right)^{-1}, \tag{A7}$$

where $L_{co} = l'_{co}l''_{ci}/(l''_{ci} + l''_{co}) = Ca^{2+}$ extracellular occlusion modulus and $L_{ni} = l'_{ni}l''_{no}e^{\Psi/2}/(l''_{ni} + l''_{no}e^{\Psi/2}) = Na^+$ cytoplasmic occlusion modulus. Here, $f_{co} = C_o/(C_o + K_{co})$ at $N_o = 0$ and $f_{3ni} = (N_i/(N_i + K_{ni}))^3$ at $C_i = 0$.

The corresponding expression for the inward turnover rate ν_i is given by

$$\nu_i = \left(\frac{1}{k_{co}} + \frac{1}{k_{ni}} + \frac{1}{l''_{co}} + \frac{1}{l''_{ni}} + \frac{2}{k_{ci}} + \frac{2}{k_{no}} + \frac{3}{f_{ci}L_{ci}} + \frac{3}{f_{3no}L_{no}}\right)^{-1}, \tag{A8}$$

where $L_{ci} = l'_{ci}l''_{co}/(l''_{ci} + l''_{co}) = Ca^{2+}$ cytoplasmic occlusion modulus and $L_{no} = l'_{no}l''_{ni}/[(l''_{ni} + l''_{no}e^{\Psi/2})e^{\Psi/2}] = Na^+$ extracellular occlusion modulus. Here, $f_{ci} = C_i/(C_i + K_{ci})$ at $N_i = 0$ and $f_{3no} = [N_o/(N_o + K_{no})]^3$ at $C_o = 0$.

This research was supported by grants from the Medical Research Council of Canada, the Heart and Stroke Foundation of Canada, and the Manitoba Health Research Foundation. The authors would like to thank Dr. Mark Hnatowich for critically reviewing the manuscript and Dr. Jonathan Wagg for providing us with LAMKIN software.

REFERENCES

Allen, T. J. A., and P. F. Baker. 1986. Comparison of the effects of potassium and membrane potential on the calcium-dependent sodium efflux in squid axons. *J. Physiol. (London).* 378:53–76.

Baker, P. F., and R. DiPolo. 1984. Axonal calcium and magnesium homeostasis. *Curr. Top. Membr. Transp.* 22:195–248.

Blaustein, M. P. 1977. Effects of internal and external cations and of ATP on sodium–calcium and calcium–calcium exchange in squid axon. *Biophys. J.* 20:79–111.

Cheon, J., and J. P. Reeves. 1988. Site density of the sodium–calcium exchange carrier in reconstituted vesicles from bovine cardiac sarcolemma. *J. Biol. Chem.* 263:2309–2315.

Cook, N. J., and U. B. Kaupp. 1988. Solubilization, purification and reconstitution of the sodium-calcium exchanger fron bovine retinal rod outer segments. *J. Biol. Chem.* 263:11,382–11,388.

Diebler, H., M. Eigen, G. Ilgenfritz, G. Maas, and R. Winkler. 1969. Kinetics and mechanism of reactions of main group metal ions with biological carriers. *Pure Appl. Chem.* 20:93–115.

DiPolo, R. 1979. Calcium influx in internally dialyzed squid giant axons. *J. Gen. Physiol.* 73:91–113.

Doering, A. E., D. A. Nicoll, J. N. Weiss, and K. D. Philipson. 1996. Effects of site-directed mutagenesis in the putative transmembrane segments on cardiac Na^+/Ca^{++} exchanger electrogenicity. *Biophys. J.* 70:7a.

Forbush, B. III. 1988. Occluded ions and Na, K-ATPase. *In* The Na, K-Pump, Part A: Molecular Aspects of Progress in Clinical Biology Research. 268A. J. C. Scou, J. G. Norby, A. B. Maunsbach, and M. Esmann, editors. Liss, New York. 229–248.

Hilgemann, D. W. 1990. Regulation and deregulation of cardiac Na^+–Ca^{2+} exchange in giant excised sarcolemmal membrane patches. *Nature (London).* 344:242–245.

Hilgemann, D. W., D. A. Nicoll, and K. D. Philipson. 1991. Charge movement during Na^+ translocation by native and cloned cardiac Na^+/Ca^{2+} exchanger. *Nature (London).* 352:715–718.

Johnson, E. A., and J. M. Kootsey. 1985. A minimum mechanism for Na^+–Ca^{++} exchange: net and unidirectional fluxes as functions of ion composition and membrane potential. *J. Membrane Biol.* 86:167–187.

Johnson, E. A., D. R. Lemieux, and J. M. Kootsey. 1992. Sodium-calcium exchange: derivation of a state diagram and rate constants from experimental data. *J. Theor. Biol.* 156:443–483.

Kimura, I., S. Miyamae, and A. Noma. 1987. Identification of sodium–calcium exchange current in single ventricular cells of guinea-pig. *J. Physiol. (London).* 384:199–222.

King, E. L., and C. Altman. 1956. A schematic method of deriving the rate laws for enzyme-catalyzed reactions. *J. Phys. Chem.* 60:1375–1378.

Lam, C. F. 1981. Techniques for the Analysis and Modelling of Enzyme Kinetic Mechanisms. John Wiley & Sons, New York.

Lauger, P. 1972. Carrier-mediated ion transport. *Science.* 178:24–30.

Lauger, P. 1987. Voltage dependence of sodium–calcium exchange: predictions from kinetic models. *J. Membrane Biol.* 99:1–11.

Lauger, P. 1991. Electrogenic Ion Pumps. Sinauer Associates, Inc., Sanderland, MA.

Ledvora, R. F., and C_{3} Hegyvary. 1983. Dependence of Na^+–Ca^{2+} exchange and Ca^{2+}–Ca^{2+} exchange on monovalent cations. *Biochim. Biophys. Acta.* 729:123–136.

Markin, V. S., and Yu. A. Chizmadjev. 1974. Induced Ion Transport. Nauka, Moscow.

Matsuoka, S., and D. W. Hilgemann. 1992. Ion and voltage dependencies of the transport cycle. *J. Gen. Physiol.* 100:963–1001.

Nicoll, D. A., and M. L. Applebury. 1989. Purification of the bovine rod outer segment Na^+–Ca^{2+} exchanger. *J. Biol. Chem.* 264:16,207–16,213.

Niggli, E., and W. J. Lederer. 1991. Molecular operations of the sodium–calcium exchanger revealed by conformation currents. *Nature (London).* 349:621–624.

Philipson, K. D., and D. A. Nicoll. 1993. Molecular and kinetic aspects of sodium-calcium exchange. *Int. Rev. Cytol.* 137C:199–227.

Post, R. L., C. Hegyvary, and S. Kume. 1972. Activation by adenosine triphosphate in the phosphorylation kinetics of sodium and potassium ion transport adenosine triphosphatase. *J. Biol. Chem.* 247:6530–6540.

Powell, T., A. Noma, T. Shioya, and R. Z. Kozlowski. 1993. Turnover rate of the cardiac Na^+–Ca^{2+} exchanger in guinea-pig ventricular myocytes. *J. Physiol. (London).* 472:45–53.

Requena, J. 1978. Calcium efflux from squid axons under constant electrochemical gradient. *J. Gen. Physiol.* 72:443–470.

Tanford, C. 1961. Physical Chemistry of Micromolecules. John Wiley & Sons, New York.